Vol. 31, No. 3
Journal of Functional Materials and Devices Jun., 2025

DOI: 10.20027/j.gncq.2025.0021 CSTR: 32180.14.j.gncq.2025.0021

Advances in atmospheric-pressure particle atomic layer deposition

YAN Guanghui[1, *], HUANG Gaoshan[1, 2, 3], LU Xueqiang[1, 4], ZUO Xueqin[3, 4], MI Dongdong[4], CHEN Guoxiang[1], OUYANG Yi[1], CHEN Xiangzhong[1, 2], BAO Zhihao[1], MEI Yongfeng[1, 2, 3], SHI Jianjun[1, 2, *]

(1. Yiwu Research Institute, Fudan University, Yiwu 322000, China; 2. International Institute for Intelligent Nanorobots and Nanosystems, Fudan University, Shanghai 200438, China; 3. Department of Materials Science, Fudan University, Shanghai 200438, China; 4. Jiangsu MNT Micro and Nanotech Co., LTD, Wuxi 214112, China)

Abstract: Atmospheric-pressure particle atomic layer deposition technology is a technique for precise modification of the surface of functional powder materials with nanoscale thickness under atmospheric pressure or near-atmospheric pressure conditions, and has broad application prospects in fields such as energy materials and catalyst materials. This technology does not require a vacuum system, significantly reducing equipment costs and maintenance costs, thus showing obvious advantages in industrial scale-up production. This paper introduces the principle of self-limiting surface chemical reactions in powder atomic layer deposition, analyzes the technical difficulties to be overcome, as well as its advantages and disadvantages, outlines the conformality characteristics of atomic layer deposition, summarizes the design methods of temporal and spatial atomic layer deposition reaction chambers under atmospheric pressure and their differences in high-throughput powder processing, discusses the applications of atmospheric-pressure powder atomic layer deposition in catalysis, drug delivery, lithium batteries and other fields, and looks forward to possible future research directions.

Key words: particle atomic layer deposition; atmospheric pressure; spatial atomic layer deposition; temporal atomic layer deposition; nanopowder; conformality

0 Introduction

Powder materials, especially nano-powder materials with particle sizes less than 100 nm, exhibit special chemical, physical, and biological properties due to their small size and large specific surface

Fund projects: National Science and Technology Tackling Program (No. 2021YFA0715302); National Natural Science Foundation of China (No. 12475259; No. 62375054); Shanghai Science and Technology Commission Project (No. 21142200200; No. 22ZR1405000).
*Corresponding authors:
YAN Guanghui (1985—), male, Ph.D., associate researcher, main research direction: atomic layer deposition technology and its applications (E-mail: yangh@ywfudan.cn).
SHI Jianjun (1976—), male, Ph.D., professor, main research direction: plasma discharge and semiconductor processes (E-mail: shijianjun@ywfudan.cn).

area, and have important applications in fields such as lithium battery materials, energetic materials, pollutant degradation, ultraviolet protection, drug delivery, and magnetic resonance imaging[1-3]. To adapt nano-powder materials to special application scenarios, their surfaces usually need appropriate modification. Traditional wet chemical deposition methods involve liquid phases, resulting in long drying processes; chemical vapor deposition (CVD) methods are difficult to achieve nanoscale thickness modification of film surfaces; physical methods (such as physical vapor deposition) also cannot achieve ideal surface modification effects on nano-powder materials due to physical effects during deposition[4]. As a special vapor deposition technology, atomic layer deposition (ALD) has good conformality when processing three-dimensional complex structures (such as powders) and can achieve atomic-level thickness control. Therefore, in recent years, particle atomic layer deposition (PALD) technology and its applications have become research hotspots.

Traditional ALD (including PALD) processes are usually carried out under low vacuum conditions, which requires the use of a vacuum system to maintain the pressure environment required for ALD operation. The use of a vacuum system not only increases equipment costs but also increases maintenance costs due to the complexity of the equipment pipeline system. In view of this, an ALD technology that can work at atmospheric or near-atmospheric pressure—atmospheric-pressure particle atomic layer deposition (AP-PALD) technology—has received extensive attention. However, atomic layer deposition on powder samples at atmospheric pressure faces many challenges. For example, it is necessary to overcome the mutual attraction between particles to achieve effective dispersion of powders; the high specific surface area of powders requires sufficient precursor dosage and long enough cleaning time; and the problem of conformal deposition on three-dimensional complex structure powders also needs to be solved. Therefore, this paper first outlines the basic principle of atomic layer deposition, then introduces the difficulties and challenges faced by applying atomic layer deposition technology on powder substrates, further discusses the advantages and disadvantages of atmospheric-pressure powder atomic layer deposition, and summarizes its conformal deposition. In addition, this paper also summarizes the research progress in AP-PALD reaction chamber design and its applications, and finally looks forward to possible future research directions of this technology.

1 Fundamentals of atomic layer deposition

ALD is a special CVD method, but there is a significant difference in the input mode of reaction precursors between the two. In the CVD process, reaction precursors are input into the reaction chamber simultaneously and undergo chemical reactions on the sample surface; while in the ALD process, precursor pulses are input alternately, and the pulses are separated by cleaning steps. The cleaning gas usually uses inert gases such as N_2 and Ar.

A complete ALD process includes 4 steps, and a typical ALD process is shown in Fig. 1[5]: (1) Precursor A is pulsed and completely covers the sample surface. (2) Cleaning step: inert gas is used to remove excess precursor A. (3) Precursor B is pulsed and undergoes a self-limiting chemical reaction with precursor A on the sample surface. (4) Cleaning step: inert gas is used to remove reaction by-products and excess precursor B. Steps (1)-(4) form a cycle, and the growth rate of the ALD process is usually described by the film deposition thickness after one cycle (Growth Per Cycle,

GPC). The growth rate of a single cycle is generally less than 1 monolayer (ML) thickness, usually 30%-50% of ML[5-6], which is related to factors such as the steric hindrance effect of precursor groups and the density of active sites on the substrate surface. The total film deposition thickness can be precisely controlled by the number of cycles, and the film control accuracy of ALD reactions can reach the atomic level.

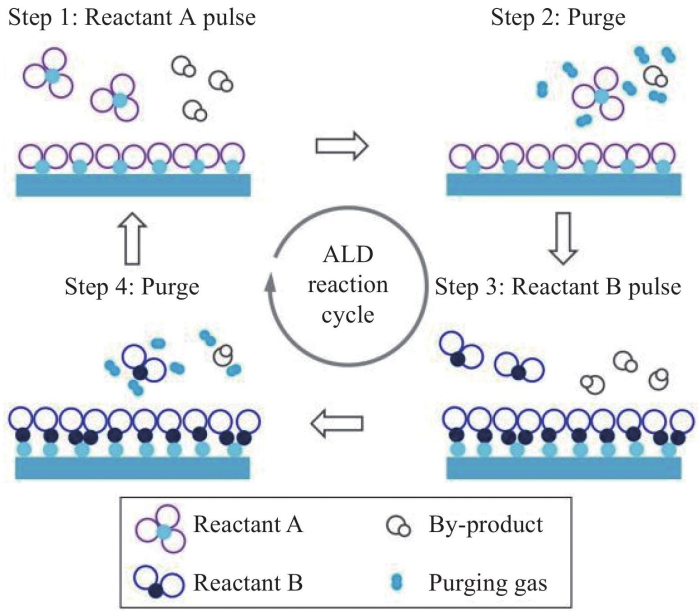

Fig. 1 Schematic diagram of a typical ALD reaction process[5]

The entire ALD reaction can be regarded as consisting of 2 separate "half-reactions". Taking the deposition process of Al_2O_3 films (using trimethylaluminum (TMA) and water as precursors) as an example, the 2 "half-reactions" can be expressed by the following reaction equations[5, 7]:

$$AlO\ H^* + Al(CH_3)_3\ (g) \rightarrow AlOAl(CH_3)_2^* + CH_4\ (g) \quad (1)$$

$$AlCH_3^* + H_2O\ (g) \rightarrow AlO\ H^* + CH_4\ (g) \quad (2)$$

In the above reactions, * represents surface groups. In half-reaction (1), the hydroxyl group (—OH) on the substrate surface is converted to a methyl group ($—CH_3$); in half-reaction B, the $—CH_3$ on the substrate surface is converted back to —OH, and finally Al_2O_3 solid is generated on the substrate surface with the release of CH_4 gas. For the deposition of Al_2O_3 materials, hydroxylation of the substrate surface is helpful for the initiation of ALD reactions.

Studies have shown that the influence of the surface chemical properties of the substrate on the ALD reaction varies with the type of substrate, which is particularly obvious in the initial stage of the ALD reaction, and the deposition rate of the film is also affected[5]. For powder crystals, if different crystal planes are exposed, area-selective atomic layer deposition (AS-ALD) may occur, that is, ALD reactions easily occur on some crystal planes but not on others[8].

2 Particle atomic layer deposition

PALD is a subdivision of ALD. On the one hand, the principle of PALD reactions is the same as that of planar samples, so it has both the advantages and limitations of ALD; on the other hand, it also

has its own characteristics. PALD usually deals with ultra-fine powders or nano-powders with small particles and large specific surface areas, and coating the surface of such powders with ALD is full of challenges.

2.1 Challenges faced by particle atomic layer deposition

Ultra-fine powders or nano-powders have mutual attraction caused by van der Waals forces, electrostatic forces, and liquid bridge forces, and are prone to soft agglomeration or even hard agglomeration to form clusters[4, 9-10]. The existence of clusters hinders the interaction between gas molecules and the surface of internal powder particles, thereby affecting the ALD process on the powder surface. Based on the powder particle packing model, Longrie et al.[11] studied the integrity of powder coating under fixed bed conditions. As shown in Fig. 2(a), when there are few powder particles, precursor gas molecules can easily undergo ALD reactions with the surfaces of all particles; while when the powder packing is thick (as shown in Fig. 2(b)), due to the long time required for precursor gas molecules to be transported to the bottom particles, only the surface of the particles in the upper part of the powder bed can form a coating layer, while the coating of the bottom particles is incomplete. By establishing a powder particle packing model, Longrie et al.[11] estimated that when the pressure drop of the fixed bed is 100 Pa, the time required for precursor gas molecules to completely reach the bottom of the powder bed from the top of the reaction chamber is 270 h. To ensure sufficient interaction between the powder particle surface and precursor gas molecules, effective dispersion of powder particles has become a key problem that must be solved in PALD technology. For this reason, scholars have developed various PALD reaction chambers, such as rotating beds[12] and fluidized beds[13].

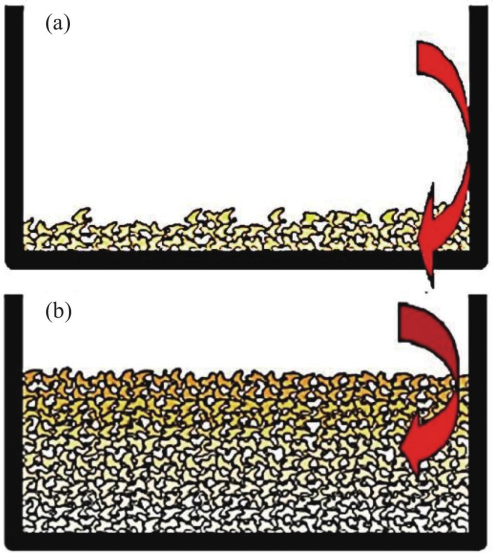

Fig. 2 Schematic diagrams of ALD coating on fixed bed particles in the cases with (a) a few particles and (b) a large amount of particles in the crucible[11]

The working pressure of traditional viscous flow reaction chambers is generally in the range of 133-1330 Pa[14]. To maintain this low-pressure environment, a vacuum system is required, and the introduction of a vacuum system not only increases equipment costs but also increases maintenance costs, which poses challenges to the large-scale production of PALD. In addition, the production

efficiency of ALD is very low, mainly because its cleaning steps are time-consuming, accounting for more than 50% of the entire standard ALD process time[15]. The demand for high efficiency in industrial production has prompted the optimization of ALD technology to a higher level. It is also worth noting that unlike planar substrates, 3D complex structure powders have high aspect ratios, and the transport of gas molecules will have a significant impact on film deposition effects. Therefore, conformal deposition of powder particles is a key issue that needs to be focused on in PALD technology.

2.2 Advantages and disadvantages of atmospheric-pressure particle atomic layer deposition

To address the challenges faced by PALD, the concept of atmospheric-pressure powder atomic layer deposition has emerged. As the name suggests, AP-PALD completes film deposition through ALD surface chemical reactions under atmospheric pressure or near-atmospheric pressure (100 kPa). The application of AP-PALD technology does not require vacuum equipment and pipelines, significantly reducing equipment and maintenance costs, and providing an economically feasible solution for large-scale production.

It can be seen from the 4 steps of the ALD process (precursor A pulse—cleaning—precursor B pulse—cleaning) that each precursor gas pulse is separated by a cleaning step, so that the 2 "half-reactions" of the ALD reaction act alternately on the sample substrate. This ALD process is called temporal atomic layer deposition (t-ALD), as shown in Fig. 3(a)[16]. Studies[7] have shown that the growth rate of Al_2O_3 films deposited on planar substrates is 0.11-0.12 nm·cycle^{-1}; while the growth rate can reach 0.14-0.20 nm·cycle^{-1} when depositing Al_2O_3 on powder substrates, which may be related to the curvature of the particles[12, 17-18]. Generally speaking, the film deposition rate of traditional planar t-ALD is 0.01-0.1 nm·s^{-1}[19]. If the 2 "half-reactions" of the ALD process act on the sample substrate simultaneously and are separated by physical isolation (such as inert gas), it constitutes spatial atomic layer deposition (s-ALD), as shown in Fig. 3(b)[16]. In s-ALD, the entire ALD reaction can be completed by moving the substrate position. Poodt et al.[20] found through the establishment of a kinetic model that the film deposition rate of s-ALD is closely related to $\sqrt{t}$ (t is time). Under appropriate temperature and saturated deposition conditions, the film deposition rate can be significantly increased to 1-10 nm·s^{-1}. Therefore, s-ALD that can work at atmospheric pressure has become a research hotspot[19, 21-22].

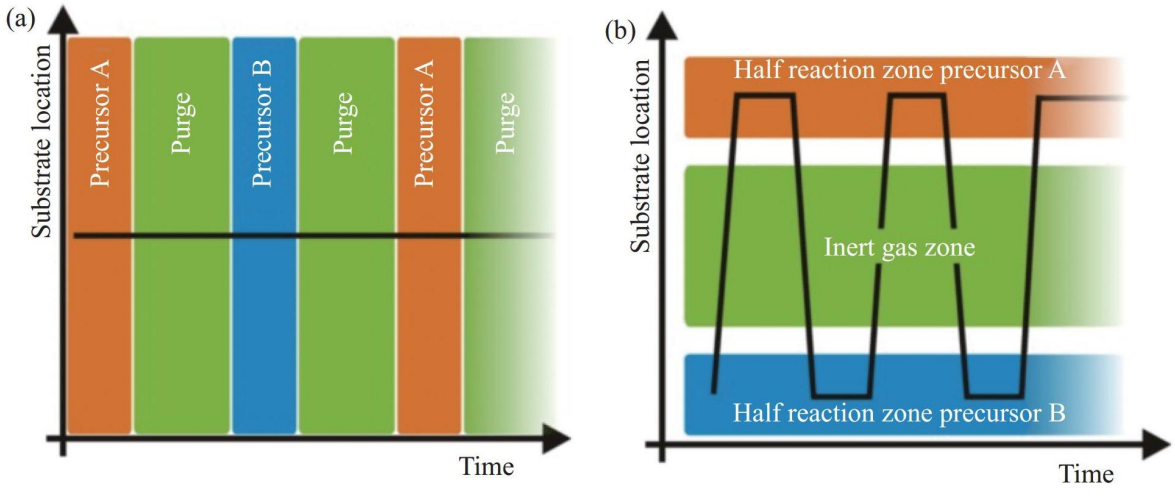

Fig. 3 Schematic diagrams of t-ALD and s-ALD processes[16]. (a) t-ALD process; (b) s-ALD process

Although AP-PALD has advantages such as low equipment cost, low maintenance cost, and fast deposition rate, it still has some shortcomings. (1) In an atmospheric pressure environment, the mean free path of gas molecules is significantly smaller than that under low pressure conditions. Although the gas pulse time can be reduced by increasing the gas molecule flux, for micro-nano slender pores formed by powders, the transport time of gas molecules in the slender pores will be prolonged due to Knudsen diffusion[21]. (2) The working pressure of AP-PALD is high, and high vapor pressure precursors such as TMA and diethylzinc (DEZ) can be smoothly transported to the reaction chamber; but for precursors with low volatility, conventional input methods face difficulties, which limits the types of precursors. (3) For atmospheric pressure s-ALD reaction chambers, especially proximity s-ALD reaction chambers, the distance between the precursor nozzle and the moving substrate is very small (only 100-200 μm)[16], which is prone to problems such as precursor nozzle blockage. (4) When the ALD reaction is operated at atmospheric pressure, oxygen and water vapor in the air will affect the reaction[19], especially for air-sensitive powders, their performance may change due to contact with air. (5) Since atmospheric pressure PALD usually operates in an open environment, the exhaust gas generated by the reaction may leak, polluting the indoor or outdoor environment.

3 Research progress on atmospheric-pressure particle atomic layer deposition

In recent years, a series of important progress has been made in the research on AP-PALD, mainly reflected in the conformality, reaction chamber design, and applications of AP-PALD.

3.1 Conformality of atmospheric-pressure atomic layer deposition

One of the advantages of ALD is its ability to form uniform films on the surfaces of high-aspect-ratio structures (including sharp corner regions), thus showing excellent conformality. For conformal deposition of high-aspect-ratio structures, Cremers et al.[23] systematically summarized model analysis and modeling. The theory of conformal deposition of high-aspect-ratio structures is of great significance for understanding the conformal deposition of powder materials.

The conformal deposition process of PALD involves the transport of gas molecules at the reaction chamber scale and powder cluster scale, as well as chemical reactions at the molecular scale. The Knudsen number (*Kn*) is a key parameter describing the transport of gas molecules in pores[24], and its expression is:

$$Kn = \lambda / d_p \tag{3}$$

In the formula, *Kn* is dimensionless, λ is the mean free path of gas molecules, and d_p is the pore diameter. When the mean free path of gas molecules is much larger than the pore diameter ($Kn \gg 1$), the transport of gas molecules belongs to molecular flow, and the interaction between gas molecules and the pore wall plays a dominant role, while the collision between gas molecules can be ignored. When the mean free path of gas molecules is much smaller than the pore diameter ($Kn \ll 1$), the transport of gas molecules belongs to viscous flow. In this state, the collision between gas molecules plays a dominant role, and the interaction between gas molecules and the pore wall can be ignored. In viscous flow, particles in the gas phase collide frequently, so in PALD, the viscous flow state is conducive to the interaction between precursor molecules and powder particles. There is a transition state between molecular flow and viscous flow ($Kn \approx 1$), which is called Knudsen flow.

In formula (3), the mean free path of gas molecules can be expressed as:

$$\lambda = \frac{k_B T}{\sqrt{2}\pi d^2 P} \tag{4}$$

In the formula, k_B is the Boltzmann constant, T is the temperature, d is the molecular diameter, and P is the pressure. It can be seen from formula (4) that pressure, gas molecular diameter, and temperature all affect the mean free path to a certain extent. According to this formula, the relationship between the mean free path and gas pressure for different gas molecular diameters is calculated as shown in Fig. 4. According to the working pressure, fluids can be divided into three types: vacuum type (10^{-3}-10^{0} Pa), flow type (about 100 Pa), and atmospheric pressure type (about 10^{5} Pa)[23]. At sufficiently low pressure, the pore characteristic size can reach the molecular flow state at the mm-cm level; while at near-atmospheric pressure (such as 100 kPa), only nano-scale pores can reach the molecular flow state.

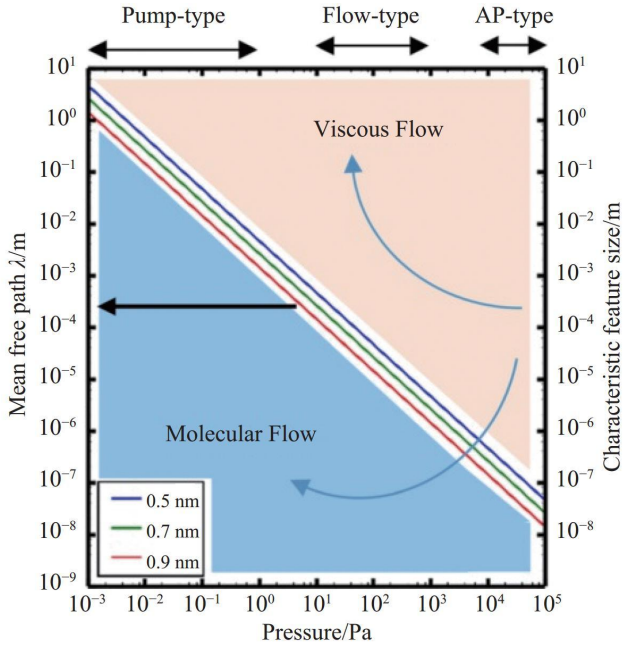

Fig. 4 Mean free path as a function of reactor pressure for three molecules with different diameters of 0.5 nm, 0.7 nm, and 0.9 nm at 100 ℃, along with the flow types determined by mean free path and characteristic feature size[23]

For clusters formed by ultra-fine powders or nano-powders, their inner surfaces can be regarded as pores with high-aspect-ratio structures. The precursor exposure required for precursor gas molecules to completely cover the substrate surface is called the saturation dose, which is the product of the precursor gas partial pressure P and its exposure time t, with the unit of Pa·s. When describing adsorption, its unit can be expressed in Langmuir (L), 1 L = 1.33×10^{-4} Pa·s. Gordon et al.[25] estimated that the saturation dose for depositing HfO_2 on planar substrates using $Hf(NMe_2)_4$ as the precursor at 200 ℃ is 3-43 L. For high-aspect-ratio materials and large specific surface area powder materials, a sufficiently large saturation dose is a necessary condition for achieving PALD conformal deposition. Based on the assumption that the adsorption coefficient of precursor gas molecules on the substrate is 1 (adsorption can cause surface reactions), Gordon et al.[25] gave the saturation dose calculation formula for the cylindrical pore wall:

$$P \cdot t = S\sqrt{2\pi m k_B T}[4a + (3/2)a^2] \quad (5)$$

In the formula, S, m, and a are the saturated adsorption surface density of precursor gas molecules, the molar mass of precursor molecules, and the aspect ratio of cylindrical pores, respectively. $S\sqrt{2\pi m k_B T}$ is the saturation dose of precursor molecules required for planar substrates. It can be seen from formula (5) that the saturation dose is closely related to the aspect ratio. Ylilammi et al.[26] studied the expansion of ALD films in lateral high-aspect-ratio pores based on the gas diffusion equation. Yazdani et al.[27] and Cremers et al.[28] studied the conformal deposition of carbon nanotubes and microcolumn arrays, respectively.

The PALD process involves both macro flow of fluids at the reaction chamber scale (such as molecular flow, Knudsen flow, and viscous flow) and gas diffusion and mass transfer processes at the cluster scale. Based on different reaction chamber pressures, precursor molecules have two diffusion modes: molecular diffusion and Knudsen diffusion. Knudsen diffusion corresponds to the case where the mean free path of gas molecules is much larger than the pores, and molecular diffusion refers to the mass transfer process formed by the irregular thermal motion of gas molecules.

Poodt et al.[29] used the effective diffusion coefficient D_{eff} to represent the contribution of molecular diffusion D_{M} and Knudsen diffusion D_{Kn} to the gas molecular diffusion process, and its expression[29-30] is:

$$D_{\text{eff}} = \left(\frac{1}{D_{Kn}} + \frac{1}{D_{\text{M}}}\right)^{-1} \quad (6)$$

Based on this, the effective diffusion coefficient curve of TMA precursor molecules was calculated. As shown in Fig. 5(a), under near-atmospheric pressure conditions, the diffusion of TMA is controlled by Knudsen diffusion when the pore diameter is less than 0.5 μm, and by molecular diffusion when the pore diameter is greater than 0.5 μm. When the pore is fixed at 1 μm, it can be seen from the relationship between the diffusion curve of TMA and the reaction chamber pressure (Fig. 5(b)) that when the reaction chamber pressure is less than 10 kPa, the diffusion of TMA is controlled by Knudsen diffusion, and the Knudsen diffusion coefficient is independent of the reaction chamber pressure. On the basis of analyzing the effective diffusion coefficient, Poodt et al.[29] derived a saturation dose expression similar to the Gordon model based on Fick's law.

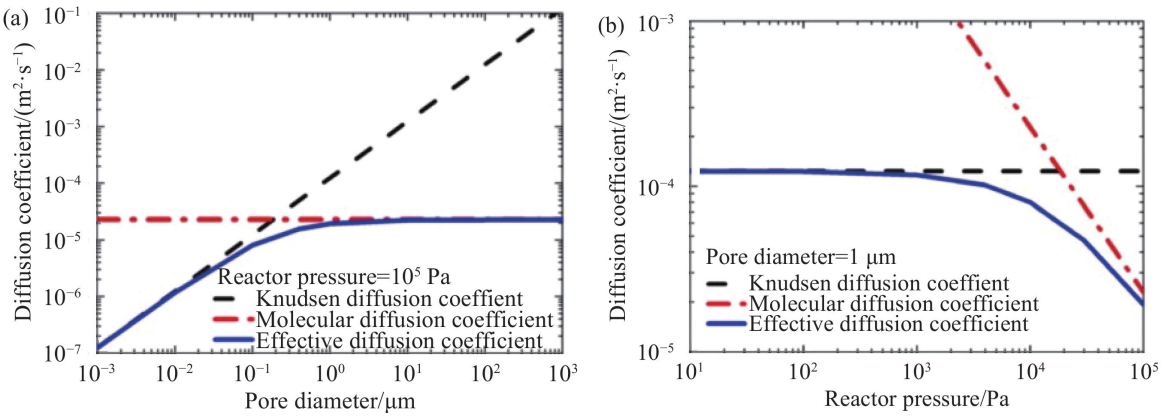

Fig. 5 (a) Diffusion coefficient of TMA as a function of pore diameter for a reactor pressure of 10^5 Pa. (b) Diffusion coefficient of TMA as a function of reactor pressure for a pore diameter of 1 μm[29]

In addition to the aspect ratio, the reaction probability between precursor gas molecules and the substrate and the diffusion coefficient also affect the saturation dose[29]. In the Gordon model[25], the adsorption coefficient is assumed to be 1. However, in the actual film deposition process, the adsorption coefficient will change with the deposition process. Inspired by the Gordon model[25], Dendooven et al.[31] further studied the influence of adsorption coefficient on film thickness based on the conductance formula. Elam et al.[32] used Monte Carlo simulation to reveal the influence of reaction probability on film deposition in high-aspect-ratio structures. Yanguas-Gil et al.[33] used the coefficient α to represent the relative ratio between the reaction rate and the diffusion rate, and obtained the relationship between the saturation dose and α, as shown in Fig. 6. For systems with low aspect ratio, low reaction probability, and high diffusion coefficient ($\alpha < 1$), the saturation dose is controlled by the reaction; while for systems with high aspect ratio, high reaction probability, and low diffusion coefficient ($\alpha > 1$), the saturation dose is controlled by diffusion.

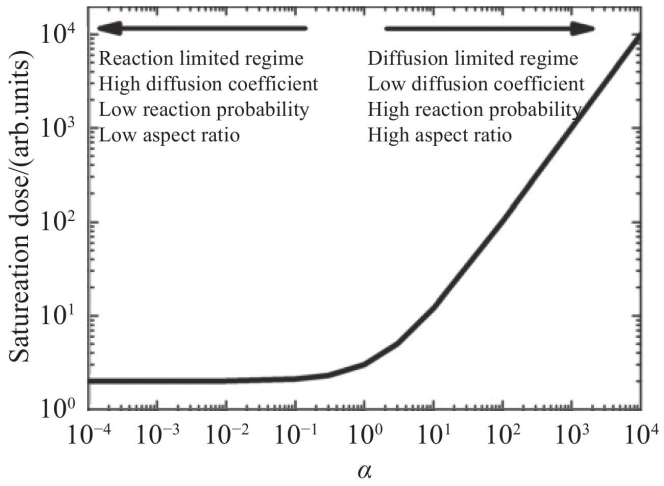

Fig. 6 Saturation dose as a function of α[33]. The reaction limited regime and diffusion limited regime can be distinguished by the α values

The reaction probabilities of Al_2O_3 and ZnO films during ALD deposition are 10^{-3} (177 ℃) and 7×10^{-3} (177 ℃), respectively, and the reaction probability of SiO_2 is as low as 10^{-8} (427 ℃)[32]. Studies[32] have shown that in high-aspect-ratio structures, the ALD deposition of SiO_2 shows reaction-controlled characteristics, while ZnO and Al_2O_3 show diffusion-controlled characteristics. It can be seen that different precursor types will affect the saturation dose of ALD deposition, thereby further affecting the conformality of film deposition. In addition, precursor types, substrates and their surface properties, and process conditions (such as temperature, pressure, etc.) may cause nucleation delay, thereby affecting the uniformity of film deposition, especially in the initial stage of film deposition (from several to dozens or even hundreds of cycles)[5, 7, 34].

In addition, temperature provides appropriate activation energy for chemical adsorption and ALD reactions, so there is a "temperature window" in ALD reactions[5]. When the temperature is higher than this "temperature window", the chemical desorption rate increases, and may lead to the decomposition of precursor gases and substrate surface species, thereby causing other additional reactions and affecting film deposition; while when the temperature is lower than this "temperature

window", it is easy to cause condensation of precursor gas molecules and incomplete surface chemical reactions, thereby affecting film deposition.

For powder ALD, different powder dispersion methods also affect the film deposition process. In fluidized bed ALD[13], the interaction between gas and powder is frequent, the mass and heat transfer efficiency is high, and the efficiency of single batch film deposition is high. For rotating bed ALD[12], there is insufficient powder dispersion, which affects the interaction between precursor gas and powder. Generally speaking, the residence time of the precursor can be increased to ensure sufficient interaction between precursor gas molecules and powder, but this method reduces the film deposition efficiency. However, the easy scale-up characteristic of rotating bed ALD makes it have unique advantages in high-throughput powder processing. It is worth noting that there are no reports on atmospheric pressure/normal pressure ALD reaction chambers based on rotating beds, which may be related to their precursor inlet methods.

3.2 Reaction chamber design

AP-PALD reaction chambers can be divided into two categories: t-ALD reaction chambers and s-ALD reaction chambers. This section introduces the design of these two types of reaction chambers respectively.

(1) t-ALD reaction chamber

In 2009, Beetstra et al.[35] designed an atmospheric pressure fluidized bed reaction chamber based on fluidized bed technology, as shown in Fig. 7(a). The reaction chamber consists of a quartz glass tube with an inner diameter of 26 mm, a height of 500 mm, and a top expansion section. The entire reaction chamber is placed on a vibrator to assist the fluidization of powder particles. To prevent the exhaust gas of different precursors from reacting in the gas washing device, two gas washing devices filled with mineral oil are connected to the gas outlet of the reaction chamber to treat the exhaust gas of different precursors. The pressure at the gas outlet is equal to atmospheric pressure.

In 2015, Soria-Hoyo et al.[36] designed an atmospheric pressure fluidized bed PALD reaction chamber without a vibrator at the bottom of the reaction chamber, as shown in Fig. 7(b). The reaction chamber consists of a quartz tube with an inner diameter of 20 mm and a height of 300 mm. O_3 is generated by an ozone generator (9), enters a gas homogenizing device (5), is uniformly mixed with N_2, and is finally carried by N_2 as a fluidizing gas to disperse nano-particles in the reaction chamber (1). The solid precursor feeding port (7) at the top of the reaction chamber is used to add glass balls attached with precursor powder into the reaction chamber. The pressure at the exhaust port (11) of the reaction chamber is atmospheric pressure.

Usually, the fluidized bed reaction chamber has a single-chamber structure. In 2021, Uğur et al.[37] designed a fluidized reaction chamber with a double-layer structure, as shown in Fig. 7(c). The first-stage fluidization chamber (9) is placed on a gas homogenizing plate with a pore diameter of 2 mm to homogenize the fluidizing gas; the second-stage fluidization chamber (11) contains the powder particles to be coated, and the powder particles are supported by a wire mesh (10) with a pore size of 212 μm. Heating wires are wound around the reaction chamber to provide the required temperature conditions for the ALD reaction. The top of the reaction chamber is connected to an exhaust gas

cleaning system (12) through a flange (8), and the pressure at the exhaust gas outlet is atmospheric pressure. The illustration at the bottom right of Fig. 7(c) is a physical diagram of the double-layer fluidized reaction chamber.

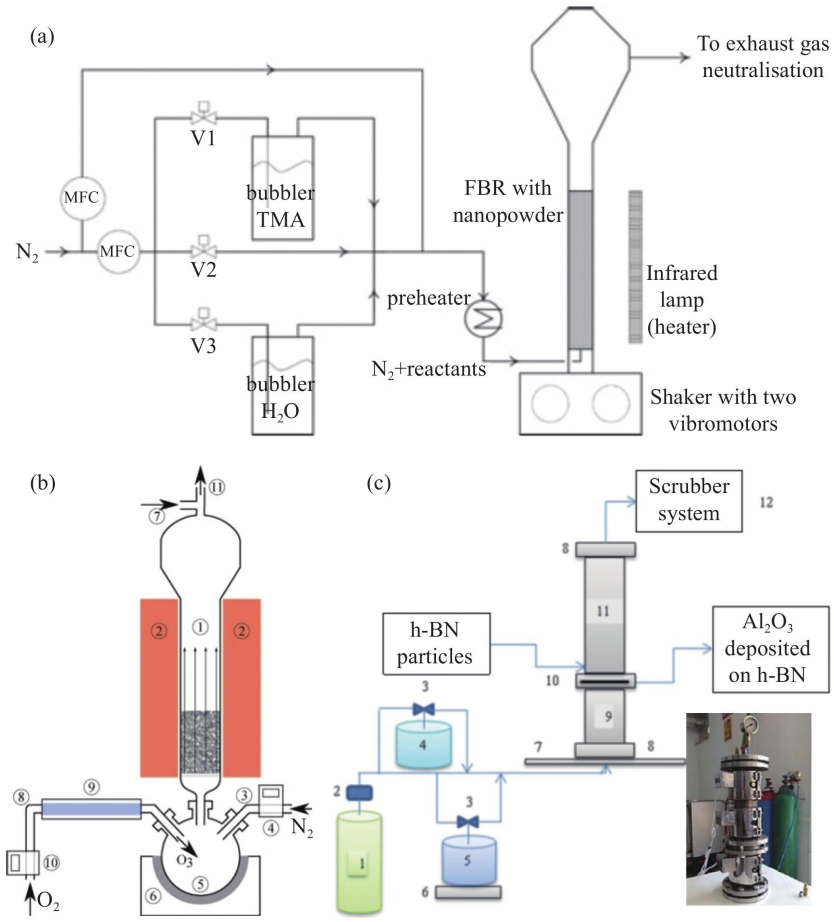

Fig. 7 (a) Schematic representation of the fluidized bed PALD reactor mounted on a vibration shaker operated at atmospheric pressure[35]. (b) Configuration of the atmospheric pressure fluidized bed ALD reactor without a vibration shaker[36]. (c) Schematic illustration of the atmospheric pressure fluidized bed reactor with double chambers[37]

The above three reaction chambers are all atmospheric pressure powder ALD reaction chambers based on fluidized bed technology, and the introduction of different precursors is time-interval, so they belong to the category of t-ALD. Fluidized reaction chambers can increase the powder loading by appropriately expanding the volume of the reaction chamber, thereby processing high-throughput powders in a batch manner. According to Forge Nano, they have expanded the volume of the fluidized bed reaction chamber to 10-20 L, but there are no reports on such large-volume reaction chambers working at atmospheric pressure.

(2) s-ALD reaction chamber

In industrial production, it is usually necessary to process hundreds to thousands of kilograms or more of powder. According to reports[38], Forge Nano has developed a rotating bed ALD equipment named "LITHOS" with a batch processing capacity of 100-1000 kg. However, from the product introduction, this equipment cannot work at atmospheric pressure. In addition to batch processing of

high-throughput powders, another high-throughput powder processing method is continuous powder processing. Continuous PALD reaction chambers that can work at atmospheric pressure are more in line with the production scale-up needs of the industrial field.

In 2015, Van Ommen et al.[39] combined powder fluidization technology with the s-ALD concept to design an s-ALD reaction chamber that can work under atmospheric pressure and process powders continuously. The reaction chamber design is shown in Fig. 8(a), mainly consisting of a feeding tank (v), a pneumatic conveying pipeline, and a powder collection tank (iv). The feeding tank transports the powder to the pneumatic conveying pipeline through gas fluidization for ALD reaction. The pneumatic conveying pipeline has a diameter of 4 mm and a length of 27 m, divided into 3 parts: preheating zone (i), precursor A conveying zone (ii), and precursor B conveying zone (iii). The powder after ALD reaction in the pneumatic conveying pipeline is finally collected in the powder collection tank (iv). This reaction chamber can realize continuous production. Due to the omission of the cleaning step in the traditional ALD process, the powder processing capacity of this s-ALD reaction chamber can reach 60 $g \cdot h^{-1}$[39]. The powder processing capacity can be further improved by appropriately expanding the pipeline volume of the pneumatic conveying s-ALD reaction chamber. Roderik Colen and others are committed to the industrialization of continuous powder processing s-ALD reaction chambers through their start-up company Powall[40].

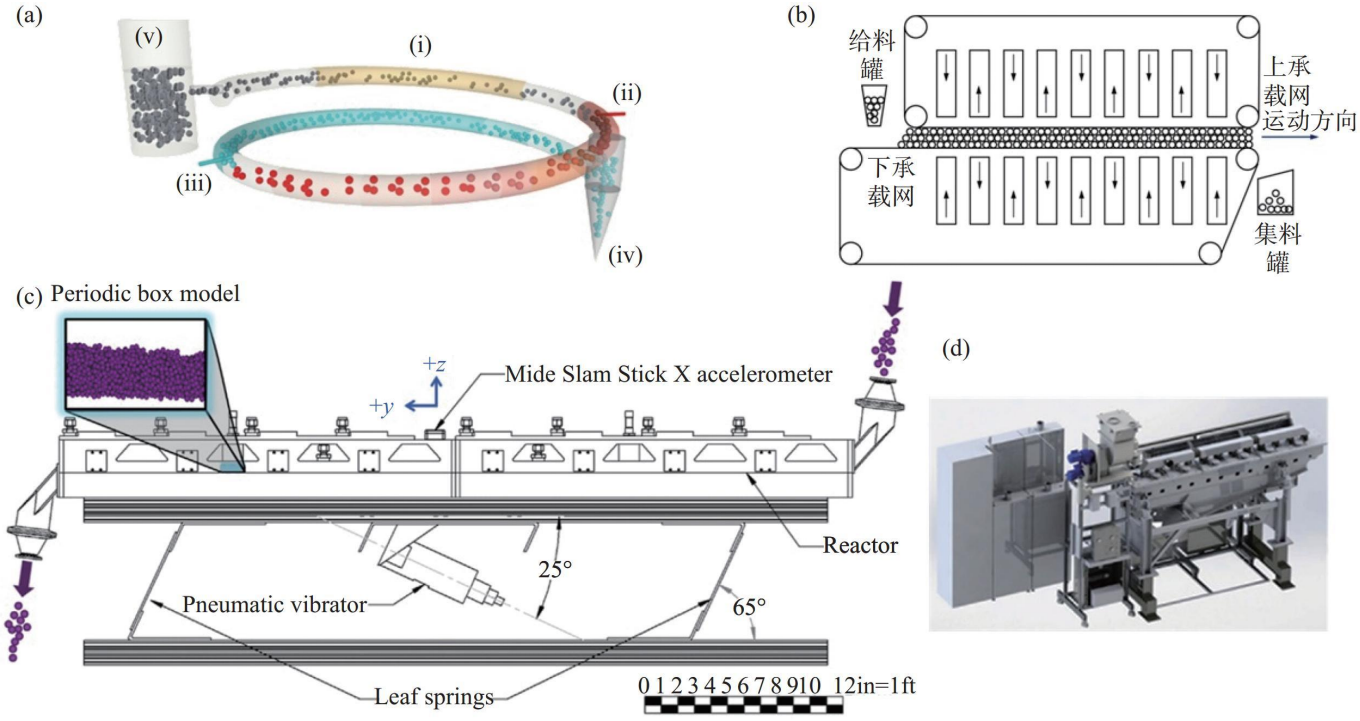

Fig. 8 (a) Schematic diagram of the pneumatic transport s-ALD reactor[39], comprising (i) pre-heating zone, (ii) reactant A reaction zone, (iii) reactant B reaction zone, (iv) collection vessel, and (v) fluidized feeding vessel. (b) Schematic diagram of the s-ALD reactor with a conveying belt[41]. (c) Schematic diagram of the vibration s-ALD reactor[43]. (d) Illustrative depiction of the vibration s-ALD system named as CIRCE[44]

Combined with the s-ALD concept, Chen Rong et al.[41] designed an s-ALD reaction chamber with a conveyor belt for powder transportation, as shown in Fig. 8(b). In this reaction chamber, the powder

to be coated is fed by a vibration motor from the feeding tank, falls on the lower carrier net with certain pores, and is transported to the reaction chamber area by a conveying device. At the end of the movement direction, a collecting tank is set to collect the coated powder particles. The powder particles to be coated are fixed by the upper and lower carrier nets in the reaction chamber area, and the contact between the powder and gas is realized by the impact of gas entering the mesh. Spencer et al.[42] designed a similar continuous s-ALD reaction chamber that relies on a conveyor belt to transport powder samples.

In addition to the above two s-ALD reaction chambers, Hartig et al.[43] from Forge Nano designed a vibration continuous s-ALD reaction chamber, as shown in Fig. 8(c). The reaction chamber relies on the vibration force provided by the vibration motor to disperse powder particles, and transports the powder particles to different precursor areas through a conveying device to complete the ALD reaction. This equipment is named "CIRCE", and its effect diagram is shown in Fig. 8(d). According to reports[44], this equipment can work at atmospheric pressure, with a powder processing capacity of up to 4000 $kg \cdot h^{-1}$ and a powder yield of 99%.

A brief comparison of the above t-ALD reaction chambers and continuous s-ALD reaction chambers working at atmospheric pressure is shown in Table 1. From the comparison results, fluidized t-ALD reaction chambers are mostly used in scientific research and small-batch experiments because of their small powder processing capacity and flexible equipment placement. Since fluidized t-ALD reaction chambers adopt batch processing of powders, it is necessary to shut down the equipment after the process is completed and frequently unload and install the reaction chamber. In contrast, continuous atmospheric pressure s-ALD does not require frequent unloading and installation of the reaction chamber, and can realize powder loading/unloading without stopping the equipment, so it has more advantages in industrial scale-up production. According to reports[40, 44], foreign companies such as Forge Nano and Powall are working hard to bring such equipment to the market.

Table 1 Comparison of different AP-PALD reactors

Reactor	ALD type	Powder dispersion	Processing method	Processing capacity	Literature
Fluidized	t-ALD	Fluidized dispersion	Batch (experiment)	<200 $g \cdot time^{-1}$	[35-37]
Pneumatic conveying	s-ALD	Gas blowing	Continuous	60 $g \cdot h^{-1}$	[39]
Conveyor belt conveying	s-ALD	Gas impact	Continuous	—	[41]
Vibration	s-ALD	Vibration dispersion	Continuous	100-4000 $kg \cdot h^{-1}$	[43-44]

3.3 Deposition structures

(1) Nano-cluster structure

Using the AP-PALD reaction chamber, Goulas et al.[45] successfully deposited Pt nano-clusters on P25 TiO_2 nano-particles at 250 ℃ and atmospheric pressure with $MeCpPtMe_3$ and ozone as

precursors. As shown in Fig. 9(a), when the number of ALD cycles is 5, the average particle size of Pt nano-clusters is 2.3 nm. Bui et al.[46] deposited Pt nano-clusters on P25 TiO_2 nano-particles at room temperature (25 ℃) and atmospheric pressure with $MeCpPtMe_3$ and O_2 as precursors. As shown in Fig. 9(b), after 5 ALD cycles, the average particle size of Pt nano-clusters is 0.5 nm. It can be seen that by adjusting the number of ALD cycles, the size of Pt nano-clusters can be precisely controlled under atmospheric pressure or even room temperature and atmospheric pressure conditions. This technology provides a precise preparation method for medium and low load noble metal catalysts and shows potential for large-scale production[47]. In addition, Van Ommen et al.[39] deposited Pt nano-clusters of about 1 nm on TiO_2 nano-particles at 100 ℃ and 250 ℃ using a continuous s-ALD reaction chamber with $MeCpPtMe_3$ and O_2 as precursors.

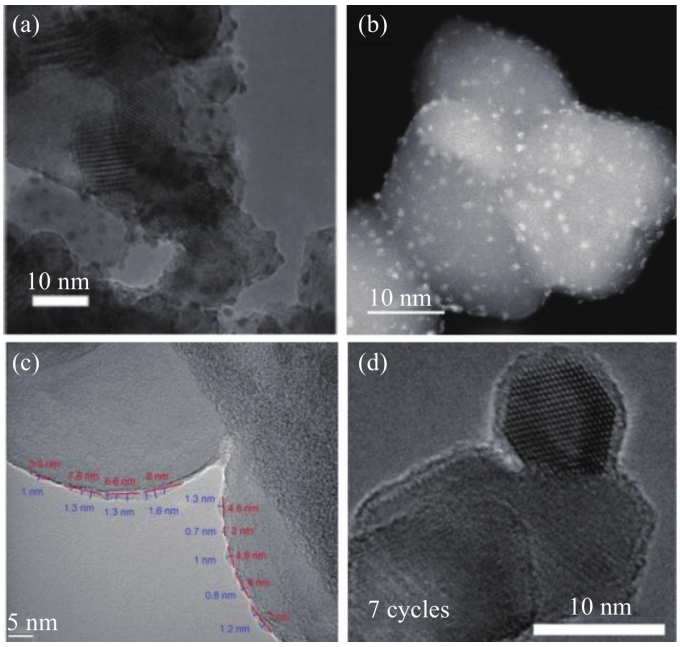

Fig. 9 (a) TEM images of 5 ALD Pt nanoclusters on P25 TiO_2 particles at 250 ℃ and atmospheric pressure, with the black dots in the TEM image representing the deposited Pt nanoclusters[45]. (b) HAADF image of Pt nanoclusters after 5 ALD cycles deposited at 25 ℃ and atmospheric pressure, with the white dots in the HAADF image representing the deposited Pt nanoclusters[46]. (c) TEM image of Al_2O_3 island film deposited on h-BN particles using an AP-PALD reactor with double chambers[37]. (d) TEM image of TiO_2 nanoparticles after 7 ALD cycles with a continuous alumina oxide film coating[36]

(2) Island structure

In addition to nano-cluster structures, island coating structures can also be deposited using AP-PALD technology. Beetstra et al.[35] carried out research on depositing Al_2O_3 on submicron (200-500 nm) lithium battery $LiMn_2O_4$ particles at 160 ℃ with TMA and H_2O as precursors. The results show that the deposited alumina film has discontinuous island structure characteristics. Uğur et al.[37] deposited Al_2O_3 on the surface of h-BN powder particles at 180-300 ℃ using a double-layer fluidized bed reaction chamber with TMA and H_2O as precursors. The results show that after 10 ALD cycles, the Al_2O_3 layer presents island coating characteristics, as shown in Fig. 9(c).

(3) Continuous film structure

Continuous film structures can also be obtained using AP-PALD technology. Valdesueiro et al.[18] deposited Al_2O_3 films on TiO_2 nano-particles at room temperature (about 27 ℃) with TMA and H_2O as precursors. Transmission electron microscopy (TEM) analysis results show that after 7 ALD cycles, the deposited Al_2O_3 film is a continuous film, as shown in Fig. 9(d), with a film growth rate of 0.14-0.15 nm·cycle^{-1}[18]. Soria-Hoyo et al.[36] mixed glass balls with a diameter of 2 mm with solid precursor $Ca(thd)_2$ to make the solid precursor powder evenly adhere to the surface of the glass balls, then added them to the fluidized reaction chamber, and filled with O_3 as a precursor to successfully realize CaO coating on the surface of nano-SiO_2 particles.

3.4 Applications

AP-PALD technology has broad application prospects in catalysis, biomedicine, energy and other fields, which are discussed in the following aspects.

(1) Catalysis field

TiO_2 has important applications in air purification, water treatment, and hydrogen production due to its excellent photocatalytic performance, high structural and chemical stability[48-49]. However, TiO_2 has some shortcomings in practical applications. On the one hand, TiO_2 has a large band gap width (about 3.2 eV) and can only absorb high-energy ultraviolet rays (200-400 nm), but cannot effectively absorb visible light and infrared rays with the highest photon flux[50]. On the other hand, photo-generated carriers are prone to recombination, which affects their photocatalytic performance[51]. To improve light absorption rate and reduce carrier recombination, Guo et al.[52] coated a nano-thick SiO_2 film on TiO_2 nano-particles using a fluidized bed PALD reaction chamber at atmospheric pressure and 100 ℃ with $SiCl_4$ and H_2O as precursors, forming a TiO_2@SiO_2 core@shell structure. It can be seen from the TEM image in Fig. 10(a) that after 8 ALD cycles, an approximately 0.7 nm thick SiO_2 film uniformly coats the TiO_2 nano-particles.

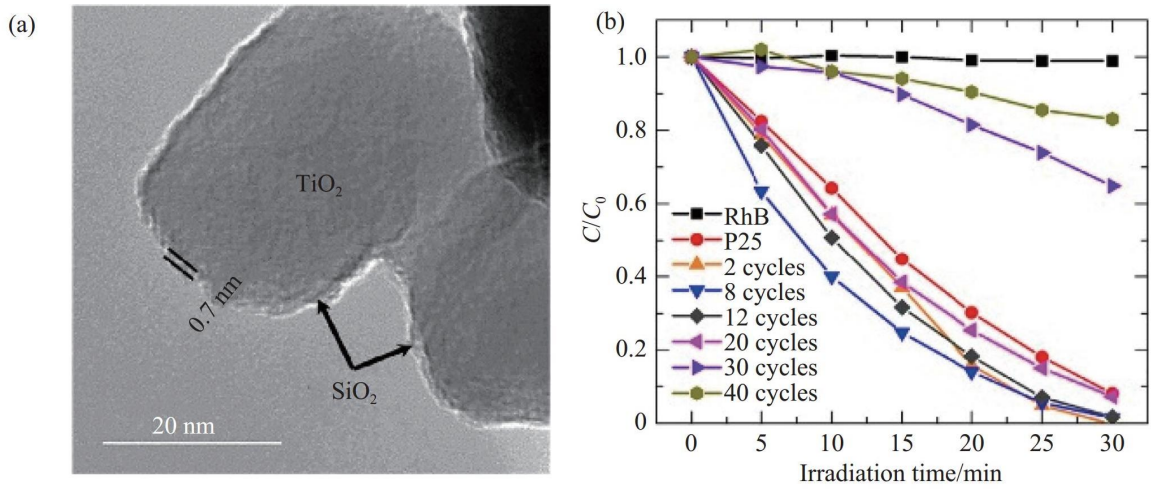

Fig. 10 (a) TEM image of the SiO_2 film deposited on TiO_2 nanoparticles after 8 ALD cycles at atmospheric pressure. (b) Degradation of RhB as a function of irradiation time for TiO_2 and ALD-coated TiO_2 nanoparticles[52]

In addition, Guo et al.[52] studied the effect of nano-TiO_2 particles coated with different ALD cycles on the photocatalytic degradation performance of rhodamine B (RhB) solution. It can be seen from Fig. 10(b) that compared with uncoated TiO_2 nano-particles and TiO_2 nano-particles coated with other ALD cycles, the TiO_2 nano-particles coated with 8 ALD cycles show the fastest degradation rate of RhB. Studies have shown that when the thickness of the SiO_2 coating is less than 1.4 nm, the photocatalytic performance of the TiO_2@SiO_2 system is enhanced, which is mainly due to the Ti—O—Si bonds formed at the interface between TiO_2 and SiO_2, which helps charge separation; while when the thickness of the SiO_2 coating is greater than 1.4 nm, the photocatalytic performance of the TiO_2@SiO_2 system is inhibited, mainly because the thick SiO_2 layer hinders the charge transport from TiO_2 to the SiO_2 layer.

Similarly, Benz et al.[53] loaded 1.3-2.0 nm thick Cu_2O nano-clusters on P25 TiO_2 nano-particles using a fluidized bed PALD reaction chamber at atmospheric pressure and 250 ℃ with Cu(I)(hfac) and H_2O as precursors to form Cu_2O/TiO_2 photocatalysts, thereby regulating the photochemical activity of TiO_2. Studies[53] found that after loading 0.4% Cu_2O, the photochemical activity of TiO_2 is the strongest, which is mainly due to the effective charge transfer between Cu_2O and TiO_2, which reduces charge recombination.

In addition, Goulas et al.[45] deposited Pt nano-clusters with a particle size range of 1.5-2.3 nm on the photocatalytic powder substrate P25 TiO_2 nano-particles using a t-ALD reaction chamber at 250 ℃ and atmospheric pressure with $MeCpPtMe_3$ and ozone as precursors. Subsequently, Van Ommen et al.[39] deposited Pt nano-clusters of about 1 nm on P25 TiO_2 nano-particles at 100 ℃ and 250 ℃ using a continuous s-ALD reaction chamber with $MeCpPtMe_3$ and O_2 as precursors. To effectively control the diffusion and aggregation during the growth of Pt nano-clusters, Bui et al.[46] deposited high-quality Pt sub-nano-clusters on P25 TiO_2 nano-particles at room temperature (25 ℃) and atmospheric pressure with $MeCpPtMe_3$ and O_2 as precursors.

In the field of carbon neutrality, using noble metal catalysts to electrochemically reduce CO_2 to intermediate products such as formic acid/formate is an effective method[54-55]. The synthesis of traditional noble metal catalysts usually requires the use of a large amount of solvents[56], and it is difficult to achieve nano-scale control of the morphology of noble metal catalysts[57]. Based on this, Li et al.[58] constructed nanostructures of Pt and Pd noble metal catalysts on carbon black substrates using atmospheric pressure fluidized bed PALD technology. Among them, Pt was deposited with $MeCpPtMe_3$ and O_3 as precursors, and Pd was deposited with $Pd(hfac)_2$ and formalin as precursors, with a deposition temperature of 200 ℃. As shown in Fig. 11(a)-(e), they prepared catalysts with Pt@Pd and Pd@Pt core@shell nanostructures and Pt-Pd bimetallic catalyst materials using AP-PALD technology. The test results of the three noble metal catalysts show that the Faraday efficiency of Pt-Pd bimetallic catalysts for formate reaches 46% (Fig. 11(f)), which is much higher than 22% of Pt@Pd (Fig. 11(b)) and 11% of Pd@Pt (Fig. 11(d)). This is mainly because the bimetallic nanostructures show higher stability in the electrochemical reduction of CO_2.

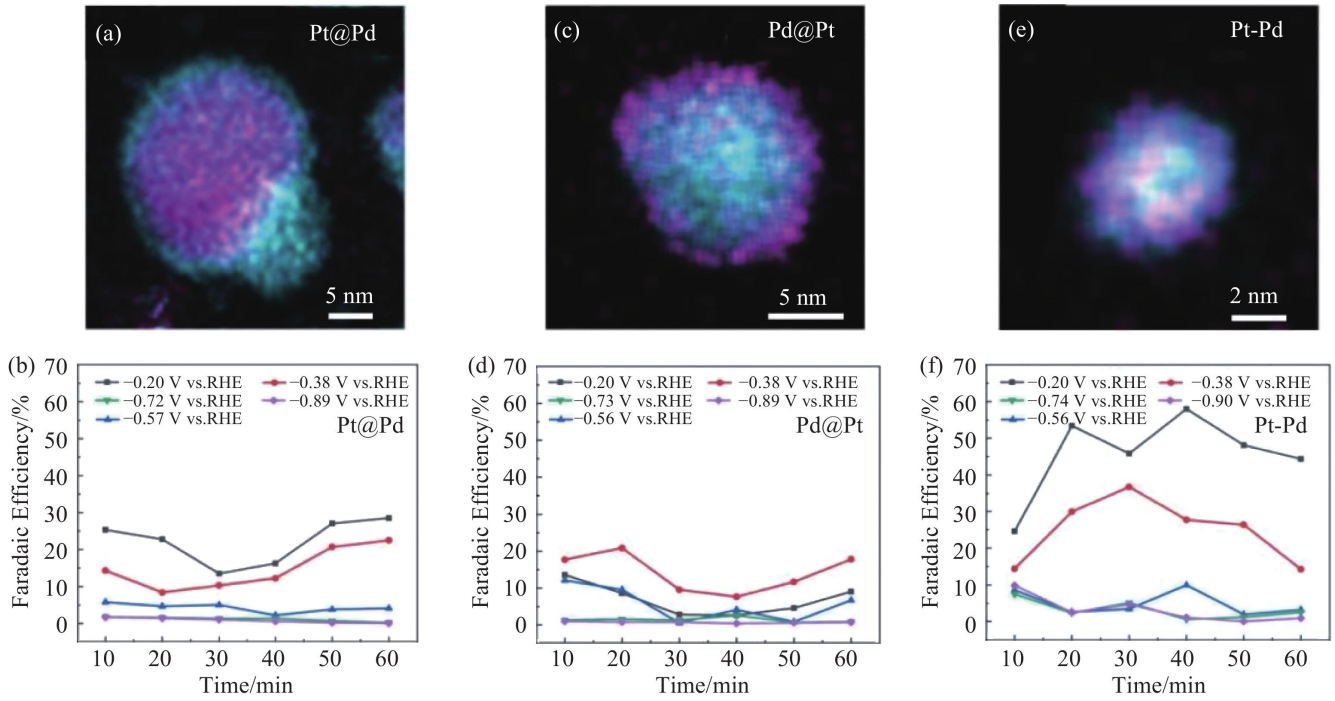

Fig. 11 (a) EDX images of Pt@Pd catalytic particle. (b) The faradaic efficiency of Pt@Pd catalyst. (c) EDX images of Pd@Pt catalytic particle. (d) The faradaic efficiency of Pd@Pt catalyst. (e) EDX images of Pt-Pd bi-metal catalytic particle. (f) The faradaic efficiency of Pt-Pd bi-metal catalyst[58]

(2) Drug delivery and sustained release

Drug particles, such as budesonide and lactose particles, are widely used in drug delivery and treatment. On the one hand, these drug powder particles need to have controlled release characteristics; on the other hand, because they are highly adhesive and easily affected by humidity and temperature, making them difficult to disperse, it is necessary to properly coat their surfaces under low temperature conditions. Zhang et al.[59] coated Al_2O_3 nano-films on the surfaces of budesonide drug particles and lactose particles using a vibration-assisted fluidized bed reaction chamber at room temperature and 100 kPa with TMA and water as precursors, as shown in Fig. 12(a)-(b). Due to the alumina film hindering the interaction between drug particles and the external environment, the solubility of the coated drug particles is reduced, as shown in Fig. 12(c)-(d). Subsequently, Zhang et al.[60] deposited Al_2O_3 on lactose particles with average particle sizes of 3.5 μm and 21 μm at 30 ℃ and 100 kPa using TMA, water, and O_3 as precursors. The results show that the nanonization of the lactose surface enhances its sustained release effect, which is beneficial to drug delivery.

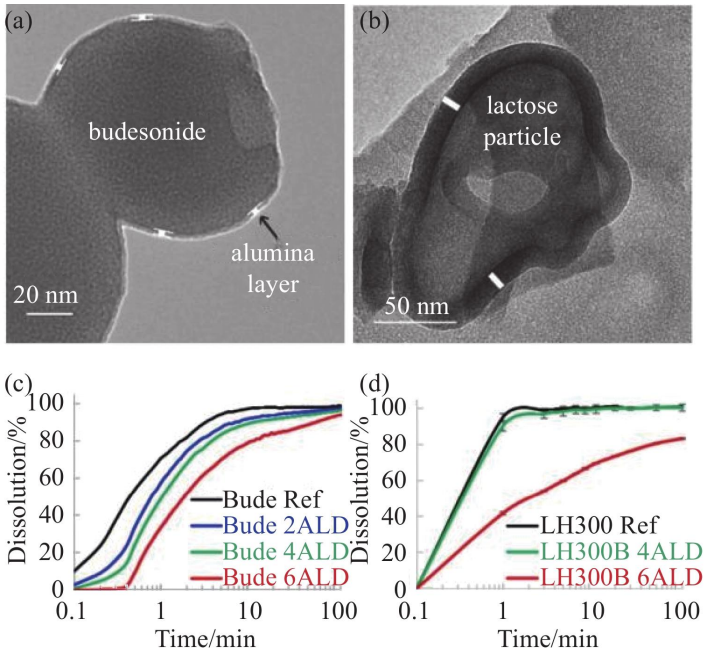

Fig. 12 TEM images of Al_2O_3 nanofilms deposited on the surfaces of (a) budesonide and (b) lactose particles by AP-PALD technology. Dissolution curves of (c) budesonide and (d) lactose after different ALD coating cycles[59]

La Zara et al.[61] compared the effects of inorganic films (Al_2O_3, TiO_2, and SiO_2) grown by AP-PALD, organic films (PET) grown by molecular layer deposition (MLD), and organic-inorganic hybrid titanicone films grown by ALD/MLD composite method on the surface wettability of budesonide drug particles (particle size 0.1-10 μm). Al_2O_3, TiO_2, and SiO_2 films were grown with TMA and O_3, $TiCl_4$ and water, $SiCl_4$ and water as precursors, respectively, and the reaction chamber temperature was 40 ℃. The research results show that the inorganic films grown by ALD can convert the hydrophobic surface of budesonide particles to hydrophilic, while the titanicone films grown by ALD/MLD composite method have mild hydrophilicity, and the PET films grown by MLD show superhydrophobicity. This indicates that the ALD method can be used to regulate the surface hydrophilicity and hydrophobicity of drug particles, which is beneficial to improve the dispersibility of drug particles in aqueous solutions.

In addition, La Zara et al.[62] used atmospheric pressure FBR-ALD technology to deposit nano-scale ceramic films (Al_2O_3, TiO_2, SiO_2) to simultaneously regulate the release characteristics and atomization characteristics of inhaled budesonide particles without using lactose carriers, thereby realizing controlled pulmonary delivery of the drug. To improve the flow characteristics of inhaled budesonide particles, Zhang et al.[63] used atmospheric pressure fluidized bed reactor-atomic layer deposition (FBR-ALD) technology to deposit ceramic films such as SiO_2, TiO_2, and Al_2O_3 on the surface of drug particles to regulate their flow performance. The results show that modifying the surface of budesonide particles with inorganic nano-films can effectively reduce the interaction force between drug particles, thereby significantly improving the delivery amount of drug particles during pneumatic transportation. Recently, Cao et al.[64] deposited SiO_2 nano-films on the surface of metformin hydrochloride particles, a drug for blood sugar control, at room temperature using atmospheric pressure FBR-ALD technology with $SiCl_4$ and H_2O as precursors. The results show that

without affecting the physical and chemical properties of metformin hydrochloride particles, SiO_2 coating reduces its dissolution rate to 1/8 of that of the uncoated sample, which plays a role in prolonging drug sustained release.

(3) Energy materials and other emerging fields

In lithium battery materials, $LiMn_2O_4$ is a cheaper cathode material than $LiCoO_2$ with high capacity and high output voltage. However, Mn ions are easily dissolved in organic electrolytes, leading to capacity loss. Coating the surface of cathode materials with Al_2O_3 can reduce their capacity loss[4, 9]. Based on this, Beetstra et al.[35] successfully coated Al_2O_3 nano-films on $LiMn_2O_4$ powder particles (particle size 200-500 nm) using AP-PALD technology with TMA and water as precursors. In addition, AP-PALD technology can also be used for CO_2 capture. Soria-Hoyo et al.[36] coated a CaO layer on the surface of SiO_2 nano-particles using their designed AP-PALD reaction chamber with $Ca(thd)_2$ and O_3 as precursors. Multi-cycle thermogravimetric analysis shows that the SiO_2 substrate can stabilize the CO_2 capture capacity of CaO.

In recent years, AP-ALD technology has also shown broad application potential in some emerging fields. In these fields, although the substrate morphology is not powder, similar to powder, they also have high aspect ratio characteristics, so they are briefly summarized here.

The core of gas chromatography lies in the capillary column. When traditional ALD technology is used to modify the inner surface of capillary columns, there are problems such as long vacuum pumping time, limited diffusion of flushing gas in the capillary, and difficulty in flushing. Patel et al.[65] designed a flow-through atmospheric pressure t-ALD reactor, in which flushing gases such as nitrogen are introduced from one end of the capillary and discharged from the exhaust port. Using this device, with TMA and H_2O as precursors, an approximately 10 nm thick Al_2O_3 nano-film was successfully coated on the inner wall of a capillary column with a length of 5-12 m and an inner diameter of 0.53 mm[65]. AP-ALD technology is also used to regulate the inner diameter of separation membrane pores and surface modification to improve the selectivity and anti-fouling ability of membrane separation. Shang et al.[66] deposited TiO_2 nano-films on the inner wall of ceramic nano-filtration membranes using a designed flow-through atmospheric pressure t-ALD reaction chamber with $TiCl_4$ and H_2O as precursors, reducing the pore diameter of the filtration membrane from 0.7 nm to 0.5 nm while maintaining high water permeability of the nano-filtration membrane. Toldra-Reig et al.[67] successfully deposited ZnO nano-coatings on the outer surface of porous alumina membranes using 3D printed s-ALD manifolds with DEZ and H_2O as precursors. Recently, Santoso et al.[68] modified the inner surface of polydimethylsiloxane (PDMS) microfluidic chips using flow-through AP-ALD technology with $SiCl_4$ and O_3, TDMAT and O_3 as precursors at reaction temperatures of 50 ℃ and 100 ℃, respectively. Studies have shown that PDMS microfluidic chips modified with nano-thick coatings show stronger resistance to organic solvent swelling and higher hydrophilicity.

The applications of AP-PALD technology (including AP-ALD technology in some non-powder substrate cases) in catalysis, biomedicine, energy materials, and other emerging fields are summarized in Table 2.

Table 2 Summary of the applications of AP-ALD technique in different areas

Material	Precursor I	Precursor II	Substrate morphology	Deposition temperature/℃	Application field	Literature
SiO_2	$SiCl_4$	H_2O	Powder	100	Photocatalysis	[52]
Cu_2O	Cu(I)(hfac)	H_2O	Powder	250	Photocatalysis	[53]
Pt	$MeCpPtMe_3$	O_3	Powder	200	Catalysis	[58]
Pt	$MeCpPtMe_3$	O_3	Powder	250	Photocatalysis	[45]
Pt	$MeCpPtMe_3$	O_2	Powder	100/250	Photocatalysis	[39]
Pt	$MeCpPtMe_3$	O_2	Powder	25	Photocatalysis	[46]
Pd	$Pd(hfac)_2$	Formalin	Powder	200	Catalysis	[58]
Al_2O_3	TMA	H_2O	Powder	40/30	Drug delivery	[59]
Al_2O_3	TMA	O_3	Powder	30	Drug delivery	[60]
Al_2O_3	TMA	H_2O	Powder	30	Drug delivery	[60]
Al_2O_3	TMA	O_3	Powder	40	Drug delivery	[61-63]
TiO_2	$TiCl_4$	H_2O	Powder	40	Drug delivery	[61-63]
SiO_2	$SiCl_4$	H_2O	Powder	40	Drug delivery	[61-63]
SiO_2	$SiCl_4$	H_2O	Powder	Room temperature	Drug sustained release	[64]
Al_2O_3	TMA	H_2O	Powder	160	Lithium battery	[35]
CaO	$Ca(thd)_2$	O_3	Powder	250	CO_2 capture	[36]
Al_2O_3	TMA	H_2O	Capillary column	300	Gas chromatography	[65]
TiO_2	$TiCl_4$	H_2O	Porous membrane	180	Water treatment	[66]
ZnO	DEZ	H_2O	Porous membrane	Room temperature	Separation	[67]
SiO_2	$SiCl_4$	Ozone	PDMS chip	50	Microfluidics	[68]
TiO_2	TDMAT	Ozone	PDMS chip	100	Microfluidics	[68]

4 Outlook

AP-PALD technology omits the vacuum system necessary in traditional low-pressure ALD technology and has significant advantages in industrial scale-up. However, there are still some aspects of this technology that need improvement and are worthy of further research in the future.

(1) Conformal growth of powder particles. Unlike planar substrates, achieving conformal coating on the surface of 3D complex structure powders involves complex gas transport processes, which requires cross-scale gas molecular transport analysis at the reaction chamber scale and powder particle scale[69-70]. Under atmospheric pressure conditions, due to the small mean free path of gas molecules, their diffusion in slender pores formed by soft agglomeration is slow. On the one hand, it

is necessary to extend the residence time of precursor gas molecules; on the other hand, it is necessary to use auxiliary means such as vibration, stirring, and jetting to effectively disperse large-capacity powders.

(2) Precursor feeding. Under atmospheric pressure conditions, the transport of precursors (especially low vapor pressure precursors) to the reaction chamber may require external force assistance such as gas pressurization.

(3) Reaction chamber design. For high-throughput powders, batch processing or continuous processing can be used. Fluidized bed AP-ALD can realize batch processing of powders. Foreign companies already have commercial 10 kg-level FBR-ALD equipment, but their working pressure is low. Therefore, the development of large-capacity fluidized bed AP-ALD equipment still faces certain technical difficulties. Compared with the batch processing method of fluidized bed t-ALD, the s-ALD system with continuous production capacity has more advantages in industrial scale-up. Therefore, the design of AP-PALD reaction chambers based on the s-ALD concept is an important development direction for future practical production. At the same time, due to the small distance between the s-ALD reaction chamber and the powder substrate, it is necessary to isolate the precursor nozzle from the powder substrate, such as using filter sheets.

(4) Environmental isolation of powder materials. For powder materials that are susceptible to oxygen or water vapor in the air, it is particularly necessary to isolate the powder materials from the above environment, such as using dry inert gases such as nitrogen to isolate the entire reaction chamber from the outside.

(5) Precursor utilization efficiency and exhaust gas treatment. In the application of AP-PALD technology, how to improve the utilization efficiency of precursors and safely and harmlessly treat the exhaust gas generated during the reaction are key issues that need to be focused on in the production field.

(6) Expansion of application fields. In the field of powder metallurgy of rare earth metal materials, the use of AP-PALD technology to uniformly coat low melting point metals on the surface of metal powders can replace the traditional method of adding low melting point metal materials through mechanical mixing[71-73]. This method is expected to improve the rheological properties of metal powders during heat treatment, thereby optimizing the microstructure of rare earth metal materials and improving their performance.

5 Summary

AP-PALD technology can precisely modify functional powder materials with nanoscale thickness under atmospheric pressure or near-atmospheric pressure, and has broad application prospects in catalysis, biomedicine, energy and other fields. This technology omits the vacuum system, saves equipment and maintenance costs, and has advantages in industrial scale-up production of functional powders. This paper first introduces the basic principles of PALD, the challenges faced by PALD technology, and the advantages and disadvantages of AP-PALD. Then, from the perspective of gas molecular transport and powder dispersion, it summarizes the conformal deposition process of PALD, summarizes the design of t-ALD and s-ALD reaction chambers suitable for atmospheric

pressure conditions, and introduces the applications of AP-PALD in catalysis, drug delivery and sustained release, batteries, and emerging fields. Finally, the possible future research directions in the field of AP-PALD are prospected. At present, AP-PALD technology and its applications have attracted great attention from researchers and engineers. With the continuous research of researchers and engineers, AP-PALD technology will play an important role in scientific research and industrial production, providing strong support for the development of related fields.

References:

[1] ALTAMMAR K. A review on nanoparticles: Characteristics, synthesis, applications, and challenges[J]. Frontiers in Microbiology, 2023, 14: 1-20.

[2] KHAN Y, SADIA H, ALI SHAH S Z, et al. Classification, synthetic, and characterization approaches to nanoparticles, and their applications in various fields of nanotechnology: A review[J]. Catalysts, 2022, 12: 1386.

[3] STARK W J, STOESSEL P R, WOHLLEBEN W, et al. Industrial applications of nanoparticles[J]. Chemical Society Reviews, 2015, 44: 5793-5805.

[4] ADHIKARI S, SELVARAJ S, KIM D H. Progress in powder coating technology using atomic layer deposition[J]. Advanced Materials Interfaces, 2018, 5: 1800581.

[5] PUURUNEN R. Surface chemistry of atomic layer deposition: A case study for the trimethylaluminum/water process[J]. Journal of Applied Physics, 2005, 97: 121301.

[6] PUURUNEN R, VANDERVORST W, BESLING W, et al. Island growth in the atomic layer deposition of zirconium oxide and aluminum oxide on hydrogen-terminated silicon: Growth mode modeling and transmission electron microscopy[J]. Journal of Applied Physics, 2004, 96: 4878-4889.

[7] GEORGE S M. Atomic layer deposition: An overview[J]. Chemical Reviews, 2010, 110: 111-131.

[8] CHEN R, GU E, CAO K, et al. Area selective deposition for bottom-up atomic-scale manufacturing[J]. International Journal of Machine Tools & Manufacture, 2024, 199: 104173.

[9] LI Z, LI J, LIU X, et al. Progress in enhanced fluidization process for particle coating via atomic layer deposition[J]. Chemical Engineering and Process, 2021, 159: 108234.

[10] SEVILLE J P K, WILLETT C D, KNIGHT P C. Interparticle forces in fluidisation: A review[J]. Powder Technology, 2000, 113: 261-268.

[11] LONGRIE D, DEDUYTSCHE D, DETAVERNIER C. Reactor concepts for atomic layer deposition on agitated particles: A review[J]. Journal of Vacuum Science and Technology A, 2014, 32: 010802.

[12] MCCORMICK J A, CLOUTIER B L, WEIMER A W, et al. Rotary reactor for atomic layer deposition on large quantities of nanoparticles[J]. Journal of Vacuum Science and Technology A, 2007, 25: 67-74.

[13] KING D M, SPENCER J A, LIANG X, et al. Atomic layer deposition on particles using a fluidized bed reactor with in situ mass spectrometry[J]. Surface & Coatings Technology, 2007, 201: 9163-9171.

[14] SCHUISKY M, ELAM J, GEORGE S. In situ resistivity measurements during the atomic layer deposition of ZnO and W thin films[J]. Applied Physics Letters, 2002, 81: 180-182.

[15] MUÑOZ-ROJAS D, MAINDRON T, ESTEVE A, et al. Speeding up the unique assets of atomic layer deposition[J]. Materials Today Chemistry, 2019, 12: 96-120.

[16] POODT P, CAMERON D C, DICKEY E, et al. Spatial atomic layer deposition: A route towards further industrialization of atomic layer deposition[J]. Journal of Vacuum Science and Technology A, 2012, 30: 010802.

[17] FERGUSON J D, WEIMER W, GEORGE S M. Atomic layer deposition of ultrathin and conformal Al_2O_3 films on BN particles[J]. Thin Solid Films, 2000, 371: 95-104.

[18] VALDESUEIRO D, MEESTERS G, KREUTZER M, et al. Gas-phase deposition of ultrathin aluminium oxide films on nanoparticles at ambient conditions[J]. Materials, 2015, 8: 1249-1263.

[19] MUÑOZ-ROJAS D, NGUYEN V, MASSE DE LA HUERTA C, et al. Spatial atomic layer deposition （SALD）, an emerging tool for energy materials. Application to new-generation photovoltaic devices and transparent conductive materials[J]. Comptes Rendus Physique, 2017, 18: 391-400.

[20] POODT P, VAN LIESHOUT J, ILLIBERI A, et al. On the kinetics of spatial atomic layer deposition[J]. Journal of Vacuum Science and Technology A, 2013, 31: 01A108.

[21] CHEN M, NIJBOER M, KOVALGIN A, et al. Atmospheric-pressure atomic layer deposition: Recent applications and new emerging applications in high-porosity/3D materials[J]. Dalton Transactions, 2023, 52: 10254-10277.

[22] MUÑOZ-ROJAS D, MACMANUS-DRISCOLL J. Spatial atmospheric atomic layer deposition: A new laboratory and industrial tool for low-cost photovoltaics[J]. Materials Horizons, 2014, 1: 314-320.

[23] CREMERS V, PUURUNEN R, DENDOOVEN J. Conformality in atomic layer deposition: Current status overiew of analysis modelling[J]. Applied Physics Reviews, 2019, 6: 021302.

[24] KNUDSEN M. Die gesetze der molekularströmung und der inneren reibungsströmung der gase durch röhren[J]. Annalen der Physik, 1909, 333: 75-130.

[25] GORDON R, HAUSMANN D, KIM E, et al. A kinetic model for step coverage by atomic layer deposition in narrow holes or trenches[J]. Chemical Vapor Deposition, 2003, 9: 73-78.

[26] YLILAMMI M, YLIVAARA O M E, PUURUNEN R L. Modeling growth kinetics of thin films made by atomic layer deposition in lateral high-aspect-ratio structures[J]. Journal of Applied Physics, 2018, 123: 205301.

[27] YAZDANI N, CHAWLA V, EDWARDS E, et al. Modeling and optimization of atomic layer deposition processes on vertically aligned carbon nanotubes[J]. Beilstein Journal of Nanotechnology, 2014, 5: 234-244.

[28] CREMERS V, GEENEN F, DETAVERNIER C, et al. Monte carlo simulations of atomic layer deposition on 3D large surface area structures: Required precursor exposure for pillar- versus hole-type structures[J]. Journal of Vacuum Science and Technology A, 2017, 35: 01B115.

[29] POODT P, MAMELI A, SCHULPEN J, et al. Effect of reactor pressure on the conformal coating inside porous substrates by atomic layer deposition[J]. Journal of Vacuum Science and Technology A, 2017, 35: 021502.

[30] O'HANLON J, GESSERT T. A user's guide to vacuum technology[M]. 4th ed. Hoboken: John Wiley & Sons, 2023.

[31] DENDOOVEN J, DEDUYTSCHE D, MUSSCHOOT J, et al. Modeling the conformality of atomic layer deposition: The effect of sticking probability[J]. Journal of the Electrochemical Society, 2009, 156: P63-P67.

[32] ELAM J W, ROUTKEVITCH D, MARDILOVICH P P, et al. Conformal coating on ultrahigh-sspect-ratio nanopores of anodic alumina by atomic layer deposition[J]. Chemistry of Materials, 2003, 15: 3507-3517.

[33] YANGUAS-GIL A, ELAM J W. Self-limited reaction-diffusion in nanostructured substrates: Surface coverage dynamics and analytic approximations to ALD saturation times[J]. Chemical Vapor Deposition, 2012, 18: 46-52.

[34] LI A D. Atomic layer deposition technology: Principles and applications[M]. Beijing： Science Press， 2016.

[35] BEETSTRA R, LAFONT U, NIJENHUIS J, et al. Atmospheric pressure process for coating particles using atomic layer deposition[J]. Chemical Vapor Deposition, 2009, 15: 227-233.

[36] SORIA-HOYO C, VALVERDE J, VAN OMMEN J, et al. Synthesis of a nanosilica supported CO_2 sorbent in a fluidized bed reactor[J]. Applied Surface Science, 2015, 328: 548-553.

[37] UĞUR A, SAVACI U, AY N, et al. Growth of ultrathin Al_2O_3 islands on hBN particles by atomic layer deposition in a custom fluidized bed reactor using Al（CH_3）$_3$ and H_2O[J]. Applied Surface Science, 2021, 537: 147665.

[38] Forge Nano LITHOS equipment[EB/OL]. [2025-03-20]. https://www.atomiclayerdeposition.com/products/forgenano-circe.

[39] VAN OMMEN J R, KOOIJMAN D, DE NIET M, et al. Continuous production of nanostructured particles using spatial atomic layer deposition[J]. Journal of Vacuum Science and Technology A, 2015, 33: 021513.

[40] Powall empowdering progress[EB/OL]. [2025-03-20]. https://www.powall.com/company.

[41] CHEN R, LI J W, SHAN B, et al. Atomic layer deposition equipment and method：2021108142424[P]. 2021-12-03.

[42] SPENCER J A, HALL R A. Continuous spatial atomic layer deposition process and apparatus for applying films on particles: US201615737023[P]. 2023-12-28.

[43] HARTIG J, HOWARD H C, STELMACH T J, et al. DEM modeling of fine powder convection in a continuous vibrating bed reactor[J]. Powder Technology, 2021, 386: 209-220.

[44] Forge Nano CIRCE equipment[EB/OL]. [2024-12-24]. https://www.atomiclayerdeposition.com/products/forgenano-circe.

[45] GOULAS A, VAN OMMEN J. Atomic layer deposition of platinum clusters on titania nanoparticles at atmospheric pressure[J]. Journal of Materials Chemistry A, 2013, 1: 4647-4650.

[46] BUI H V, NGUYEN A P, DANG M D, et al. What could be the low-temperature limit of atomic layer deposition of platinum using $MeCpPtMe_3$ and oxygen?[J]. Chemical Communications, 2024, 60: 14045-14048.

[47] GOULAS A, VAN OMMEN J R. Scalable production of nanostructured particles using atomic layer deposition[J]. KONA Powder and Particle Journal, 2014, 31: 234-246.

[48] SCHNEIDER J, MATSUOKA M, TAKEUCHI M, et al. Understanding TiO_2 photocatalysis: Mechanisms and materials[J]. Chemical Reviews, 2014, 114: 9919-9986.

[49] CHEN X B, MAO S S. Titanium dioxide nanomaterials: Synthesis; properties; modifications, and applications[J]. Chemical Reviews, 2007, 107: 2891-2959.

[50] KUMAR S, DEVI L. Review on modified TiO_2 photocatalysis under UV/visible light: Selected results and related mechanisms on interfacial charge carrier transfer dynamics[J]. Journal of Physical Chemistry A, 2011, 115: 13211-13241.

[51] OHTANI B. Titania photocatalysis beyond recombination: A critical review[J]. Catalysts, 2013, 3: 942-953.

[52] GUO J, BENZ D, DOAN NGUYEN T T, et al. Tuning the photocatalytic activity of TiO_2 nanoparticles by ultrathin SiO_2 films grown by low-temperature atmospheric pressure atomic layer deposition[J]. Applied Surface Science, 2020, 530: 147244.

[53] BENZ D, NGUYEN Y, LE T L, et al. Controlled growth of ultrasmall Cu_2O clusters on TiO_2 nanoparticles by atmospheric-pressure atomic layer deposition for enhanced photocatalytic activity[J]. Nanotechnology, 2021, 32: 425601.

[54] CHEN C, KOTYK J F K, SHEEHAN S W. Progress toward commercial application of electrochemical carbon dioxide reduction[J]. Chem, 2018, 4: 2571-2586.

[55] KORTLEVER R, SHEN J, SCHOUTEN K J P, et al. Catalysts and reaction pathways for the electrochemical reduction of carbon dioxide[J]. Journal of Physical Chemistry Letters, 2015, 6: 4073-4082.

[56] VOGT C, GROENEVELD E, KAMSMA G, et al. Unravelling structure sensitivity in CO_2 hydrogenation over nickel[J]. Nature Catalysis, 2018, 1: 127-134.

[57] O'NEILL B J, JACKSON D H K, LEE J, et al. Catalyst design with atomic layer deposition[J]. ACS Catalysis, 2015, 5: 1804-1825.

[58] LI M, FU S, SAEDY S, et al. Nanostructuring Pt-Pd bimetallic electrocatalysts for CO_2 reduction using atmospheric pressure atomic layer deposition[J]. ChemCatChem, 2022, 14: e202200949.

[59] ZHANG D, QUAYLE M J, PETERSSON G, et al. Atomic scale surface engineering of micro- to nano-sized pharmaceutical particles for drug delivery applications[J]. Nanoscale, 2017, 9: 11410-11417.

[60] ZHANG D, LA ZARA D, QUAYLE M J, et al. Nanoengineering of crystal and amorphous surfaces of

pharmaceutical particles for biomedical applications[J]. ACS Applied Bio Materials, 2019, 2: 1518-1530.

[61] LA ZARA D, ZHANG F, SUN F, et al. Drug powders with tunable wettability by atomic and molecular layer deposition: From highly hydrophilic to superhydrophobic[J]. Applied Materials Today, 2021, 22: 100945.

[62] LA ZARA D, SUN F, ZHANG F, et al. Controlled pulmonary delivery of carrier-free budesonide dry powder by atomic layer deposition[J]. ACS Nano, 2021, 15: 6684-6698.

[63] ZHANG F, WU K, LA ZARA D, et al. Tailoring the flow properties of inhaled micronized drug powders by atomic and molecular layer deposition[J]. Chemical Engineering Journal, 2023, 462: 142131.

[64] CAO V P, DINH K H T, BUI P H, et al. Toward extended release of metformin by room-temperature atomic layer deposition of thin SiO_2 films[J]. Applied Surface Science, 2025, 687: 162283.

[65] PATEL D I, MAJOR G H, JACOBSEN C, et al. Flow-through atmospheric pressure-atomic layer deposition reactor for thin-film deposition in capillary columns[J]. Analytical Chemistry, 2022, 94: 7483-7491.

[66] SHANG R, GOULAS A, TANG C Y, et al. Atmospheric pressure atomic layer deposition for tight ceramic nanofiltration membranes: Synthesis and application in water purification[J]. Journal of Membrane Science, 2017, 528: 163-170.

[67] TOLDRA-REIG F, LAUSECKER C, WEBER M, et al. Custom 3D printed spatial atomic layer deposition manifold for the coating of tubular membranes[J]. ACS Sustainable Chemistry & Engineering, 2022, 10: 14112-14118.

[68] SANTOSO A, DAVID M K, BOUKANY P E, et al. Atmospheric pressure atomic layer deposition for in-channel surface modification of PDMS microfluidic chips[J]. Chemical Engineering Journal, 2024, 498: 155269.

[69] DUAN C L, ZHU P H, DENG Z, et al. Mechanistic modeling study of atomic layer deposition process optimization in a fluidized bed reactor[J]. Journal of Vacuum Science and Technology A, 2017, 35: 01B102.

[70] LIU D, VAN WACHEM B G M, MUDDE R F, et al. Characterization of fluidized nanoparticle agglomerates by using adhesive CFD-DEM simulation[J]. Powder Technology, 2016, 304: 198-207.

[71] LUO S, LU Y, ZOU Y, et al. Effect of low melting point powder doping on the properties and microstructure of sintered NdFeB magnets[J]. Journal of Magnetism and Magnetic Materials, 2021, 523: 167620.

[72] YAN G, LIU Z, XIA W, et al. Grain boundary modification induced magnetization reversal process and giant coercivity enhancement in 2:17 type SmCo magnets[J]. Journal of Alloys and Compounds, 2019, 785: 429-435.

[73] WANG Y Q, YUE M, WU D, et al. Microstructure modification induced giant coercivity enhancement in Sm（CoFeCuZr）$_z$ permanent magnets[J]. Scripta Materialia, 2018, 146: 231-235.